

# Probing the Interstellar Medium using HI absorption and emission toward the W3 HII region

Magdalen Normandeau

Astronomy Department, University of California, Berkeley, CA 94720-3411

## ABSTRACT

HI spectra towards the W3 HII complex are presented and used to probe the Galactic structure and interstellar medium conditions between us and this region. The overall shape of the spectra is consistent with the predictions of the Two-Arm Spiral Shock model wherein the gas found in the  $-40 \text{ km s}^{-1}$  to  $-50 \text{ km s}^{-1}$  range has been accelerated by some  $20 \text{ km s}^{-1}$  from its rotation curve velocity. Spin temperatures of  $\sim 100 \text{ K}$  are derived for the Local Arm gas, lower than found in a previous, similar study towards DR 7. For the interarm region, values on the order of  $300 \text{ K}$  are found, implying a negligible filling factor for the Cold Neutral Medium ( $\ll 1\%$ ). Some of the absorbing gas at velocities near  $-40 \text{ km s}^{-1}$  is confirmed to be associated with the HII regions.

*Subject headings:* Galaxy: fundamental parameters — Galaxy: structure — ISM: general — ISM: individual(W3) — ISM: HI

## 1. Introduction

While atomic hydrogen (HI), generally seen in emission, is certainly a pervasive component of the Galaxy, our knowledge of its optical depth ( $\tau$ ) and spin temperature ( $T_s$ ) close to the Galactic plane is sparse. The main reason for this is the difficulty inherent in disentangling the emission along most sight-lines (Kulkarni & Heiles 1988). Use of absorption towards extragalactic sources has proved somewhat successful but has not been entirely satisfactory at low Galactic latitudes.

The plane is peppered with bright HII regions which could potentially be used. Wendker & Wrigge (1996) studied the HI absorption spectrum towards DR 7 as seen using the Dominion Radio Astrophysical Observatory's (DRAO) Synthesis Telescope (ST) and argued for the usefulness of such observations for the determination of optical depth and spin temperature as a function of radial velocity (or distance). The authors suggested that

the careful study of many lines of sight will contribute to the quasi mapping of  $\tau$  and  $T_s$ , although for HI at velocities corresponding to gas in the proximity of the HII regions, it is important to bear in mind that some of the absorbing material may have been dissociated by the central stars, thus presenting local enhancements which are not typical of the general surroundings. This paper contributes a second line-of-sight towards a strong, extended continuum source within our galaxy: the W3 HII complex, shown in Figure 1.

The W3 region has been studied in detail repeatedly and at many frequencies (see e.g. Roberts, Crutcher & Troland 1997 for molecular line observations; Tiefttrunk et al. 1997 for a multiwavelength radio continuum study; Roelfsema & Goss 1991 for radio recombination lines; Campbell et al. 1995 for a far-infrared look at subcomponents; and Hofner & Churchwell 1997 for X-ray). It houses active star formation and can be subdivided into multiple HII regions for which the nomenclature varies somewhat with the type of observations. Table 1 defines the terminology used in this paper.

HI studies of sight-lines towards W3 have concentrated on searching for atomic gas associated with the HII regions. While the limited spatial and spectral resolution of data presented by Sullivan & Downes (1973) precluded the detection of variations in HI opacities, observations with the Nançay telescope led Crovisier et al. (1975) to conclude that the HI absorption near  $-40 \text{ km s}^{-1}$  (all velocities in this paper are with respect to the Local Standard of Rest) is due to atomic hydrogen related to W3. Read (1981) carried out a detailed study of the HI in this region in both emission and absorption; his data had similar spatial resolution to the DRAO data presented here and somewhat poorer velocity resolution ( $4 \text{ km s}^{-1}$ ). He suggested that photodissociation of molecular gas near the compact HII regions is responsible for several observed HI concentrations. Goss et al. (1983) and van der Werf & Goss (1990) used the Westerbork Synthesis Radio Telescope (WSRT) and so had better spatial resolution ( $\sim 30''$  and  $\sim 15''$ ) than obtainable with the smaller DRAO array, as well as better velocity resolution ( $1.24 \text{ km s}^{-1}$  and  $1.03 \text{ km s}^{-1}$ ), but they do not provide full visibility plane coverage and so are not sensitive to emission on all angular scales. They also concluded that much of the HI at  $\sim -40 \text{ km s}^{-1}$  is due to dissociation and delineate shells associated with various compact HII regions.

The above authors presented studies of the W3 complex itself and therefore concentrated on HI which may be related to it, i.e. their focus was the HI absorption near  $-40 \text{ km s}^{-1}$ . The present paper uses sight lines towards W3 to probe the interstellar medium between us and this HII region, evaluating optical depths and spin temperatures, and placing it in a Galactic perspective. Section 2 briefly describes the data sets which were used in this analysis. Section 3 gives an overview of the HI profiles towards W3, placing their features in the context of rotation curves and spiral shocks, as well as outlining

the method used to derive the optical depths and spin temperatures. The fourth section provides a more detailed discussion of optical depths and spin temperatures at different velocities. And finally, the last section summarises the findings.

## 2. The data

Radio continuum data at both 408 MHz and 1420 MHz, as well as 21cm spectral line data were obtained at the DRAO as part the Canadian Galactic Plane Survey (CGPS) pilot project. The pilot project covered an  $8^\circ \times 6^\circ$  area of the sky, encompassing all of the W3/W4/W5/HB3 Galactic complex. Observations were carried out in June, July, November and December of 1993. The synthesis telescope is a 7-element interferometer with four fixed and three movable antennas, each with a diameter of  $\sim 9$  m. In the course of twelve 12-hour periods, observations are taken for all baselines from 12.858 to 604.336 m by increments of 4.286 m. At 1420 MHz, the small dish size results in a field of view of 78 arcmin (at 20% attenuation of the primary beam which is approximated by a Gaussian), the longest spacing gives a spatial resolution of  $1.00 \times 1.00 \text{ csc } \delta \text{ arcmin}^2$  (EW  $\times$  NS), and the shortest baseline means that the instrument is not sensitive to structures greater than  $0.5^\circ$  in extent.

The spectral line data were collected by a 128-channel spectrometer with a channel width of  $2.64 \text{ km s}^{-1}$  and a channel separation of  $1.649 \text{ km s}^{-1}$ . The sensitivity at field centre for the ST data is 3.0 K and degrades with distance from the centre as the inverse of the primary beam. For channels where the continuum emission from W3 is strongly absorbed there are processing artefacts from W3. Information about the lowest spatial frequencies (i.e. large angular sizes) was provided by the DRAO’s 26m telescope, and as a result the images are sensitive to structures on all scales. Relevant observational parameters are outlined in Table 2. Details of the observations and data reduction are described by Normandeau et al. (1997).

Continuum emission was subtracted from the HI images. While the DRAO synthesis telescope collects continuum data at 1420 MHz using four 7.5 MHz bands, two to each side of the line frequency, the resulting image was not used to subtract the continuum. Instead an average was taken of channels where there was no apparent HI, the first and last twenty channels corresponding to velocities between  $+55$  and  $+24 \text{ km s}^{-1}$  and between  $-137$  and  $-154 \text{ km s}^{-1}$ . This allows for a more precise subtraction of the continuum emission for three reasons: 1) the DRAO spectrometers are equipped with automatic level control which adjusts the gain in order to minimise information loss due to quantization whereas the continuum system is not, and the uncertainty of the gain correction factor would decrease

the reliability of HI images; 2) the difference in bandwidth between a spectrometer channel and the continuum receiver results in differing amounts of bandwidth smearing in the images, making the subtraction of continuum sources progressively worse with distance from field centre; 3) using the end channels insures that the visibility plane coverage is identical for all the maps involved in the operation, thus allowing a more accurate subtraction of any artefacts related to strong sources. However, the continuum brightness temperature values used in the optical depth calculations (see below) were from the true continuum image.

### 3. Overview of HI spectra towards W3

The most prominent absorption features in the CGPS pilot project data are those associated with W3 which can be seen out to  $v_{\text{LSR}} = -50 \text{ km s}^{-1}$ . While the profiles towards different points within the W3 region differ significantly from each other, mostly for velocities near  $-40 \text{ km s}^{-1}$ , they all have the same global properties which are well illustrated in Figure 2. This shows the average absorption profiles associated with W3-N and W3-W for all positions where the continuum brightness temperature is greater than 50 K. As well, an average emission spectrum from forty nearby positions (see §3.1.2) is plotted.

#### 3.1. Optical depth and spin temperature

##### 3.1.1. General considerations

Spectra towards the source (“on”), which show absorption, and towards nearby positions (“off”), showing emission, can be combined to yield the optical depth and spin temperature. For the on-source spectrum,

$$T_{\text{b,on}}(v) = T_s(v) (1 - e^{-\tau_v}) + T_c e^{-\tau_v} - T_c \quad (1)$$

where  $T_c$  is the continuum brightness temperature of the background source. The dependance on frequency and therefore radial velocity,  $v$ , is indicated. The off-source spectrum is given by the first term of the above equation:

$$T_{\text{b,off}}(v) = T_s(v) (1 - e^{-\tau_v}). \quad (2)$$

Assuming that the off-spectrum has been carefully chosen to be representative of what would be seen at the position of the source if no absorption were occurring, one can solve for the optical depth:

$$\tau_v = -\ln \left( 1 - \frac{T_{\text{b,off}}(v) - T_{\text{b,on}}(v)}{T_c} \right). \quad (3)$$

Once the optical depth has been obtained from the observed spectra and continuum brightness temperature, the spin temperature can be calculated using Eq.2. It should be noted that an over- or underestimate of  $T_{b,off}$  will result in an over- or underestimate of  $\tau$ .

### 3.1.2. The case of W3

As indicated above, the off-spectrum must be carefully chosen to be representative of the on-source emission. This proves difficult for sight-lines towards W3 as there is much variation. For forty positions within a few arcminutes of W3, 20 near W3-N and 20 near W3-W as defined by their 50 K contours, being careful to avoid the image artefacts and the slight absorption associated with W3-E, for velocities ranging from  $+8 \text{ km s}^{-1}$  to  $-91 \text{ km s}^{-1}$  which includes all of the Galactic emission of note, the standard deviation was as high as 18 K, though the average deviation in both cases was  $\sim 7 \text{ K}$ . The average spectra, for W3-N and W3-W, are shown in Figure 3 which also includes the average  $\pm 1\sigma$  profiles.

For areas where the absorption is almost total, the optical depth calculation depends very sensitively on  $T_{b,off} - T_{b,on}$ . Therefore, for the present purposes, whenever the value of  $T_{b,off}(v) - T_{b,on}(v)$  came within  $2(\sigma_{off}(v) + \sigma_{on})$  of  $T_c$  it was replaced by  $T_c - 2(\sigma_{off}(v) + \sigma_{on})$  in the calculation, where  $\sigma_{off}(v)$  is the standard deviation of the appropriate off-spectrum, and  $\sigma_{on} = 3.5\text{K}/P(\theta)$ , the uncertainty at field centre for the continuum subtracted HI images adjusted for the effect of the primary beam correction. This provides a lower limit value for the optical depth. It affects approximately 36% of the values of  $\tau$  for W3-W from  $-33.51 \text{ km s}^{-1}$  to  $-50.00 \text{ km s}^{-1}$ , and  $\sim 41\%$  of those for W3-N in this same interval. Away from this deep trough, none of the values for W3-N needed to be calculated in this manner, and less than  $\sim 2\%$  of the values for W3-W at more positive velocities are affected.

The spin temperature calculations are highly dependant on the value of  $T_{b,off}$  which is the greatest source of uncertainty. Therefore, in addition to indicating limits when only limits were calculated for  $\tau$ , results for  $T_s$  will be considered trustworthy only when  $T_s > 2\sigma_{T_s}$ .

Plots of  $\tau_v$  and  $T_s(v)$  for sight lines towards W3-N and W3-W are presented in Figures 4 and 5. These were calculated using the average spectrum of all positions where the continuum emission is greater than 50 K (i.e. the on-source spectra shown in Fig. 2) and the average of 20 nearby spectra for the emission (i.e. the emission spectra shown in Fig. 3). Calculations were also done on a pixel by pixel basis for each region.

### 3.2. Main features placed in a Galactic context

There are three main absorption troughs along this line-of-sight: one corresponding to Local gas, one corresponding to the bulk of the Perseus arm and an intermediate trough centred on  $-22 \text{ km s}^{-1}$ . There is HI emission at velocities between the intermediate and Perseus arm absorption troughs, at  $v \sim -30 \text{ km s}^{-1}$ . Three different scenarios are considered to explain this and are illustrated in Figure 6.

#### 3.2.1. *Standard rotation curve without gas displacement*

One possibility does not require that any of the gas be displaced relative to the standard rotation curve, nor that the emitting gas at  $-30 \text{ km s}^{-1}$  be behind W3 (Fig. 6a).

If the opacity of the gas at  $-30 \text{ km s}^{-1}$  were low enough, there would be sufficiently little absorption for it to be noticeable. In this framework the values of  $\tau$  calculated from the observed spectra would imply spin temperatures in excess of  $10^4 \text{ K}$  for this interarm gas, higher than expected for the Warm Neutral Medium ( $T \leq 8000 \text{ K}$ , Kulkarni & Heiles 1988; direct measurements towards Cyg A by Carilli et al. (1998) yielded  $6000 \pm 1700 \text{ K}$  and  $4800 \pm 1600 \text{ K}$ ).

This feature of the spectra extends approximately from  $-24 \text{ km s}^{-1}$  to  $-33 \text{ km s}^{-1}$ . Assuming a flat rotation curve with an Oort constant  $A = 14 \text{ km s}^{-1} \text{ kpc}^{-1}$  and  $R_0 = 8.5 \text{ kpc}$ , this implies a path length of  $0.6 \text{ kpc}$  within which there is no cold neutral hydrogen. This seems unlikely considering that the average off-source emission is approximately  $55 \text{ K}$  and that there is significant absorption at more positive velocities ( $-20 \text{ km s}^{-1}$ ) which also correspond to the interarm region for the standard rotation curve.

#### 3.2.2. *Standard rotation curve with $-30 \text{ km s}^{-1}$ gas displaced*

In the most intuitive picture, the lack of absorption at  $-30 \text{ km s}^{-1}$  places the related gas behind the W3 region.

It could be argued that the  $-30 \text{ km s}^{-1}$  gas has been displaced in velocity (Fig. 6b), that it is not following the rotation curve of the Galaxy. In this case, the less negative velocity indicates that, while it is approaching us, it is receding relative to the general movement of the Galactic HI at a velocity of at least  $19 \text{ km s}^{-1}$ , as determined from the lower velocity edge of the  $-40 \text{ km s}^{-1}$  absorption trough and the upper velocity edge of the  $-30 \text{ km s}^{-1}$  trough.

### 3.2.3. TASS model, $-40 \text{ km s}^{-1}$ gas accelerated

For the Perseus arm there are known to be large deviations from the circular motion normally assumed for the Galaxy (see Roberts 1972 and references therein); the location of the optical arm and that of the radio (HI) arm as determined using a standard Galactic velocity curve do not coincide, with the radio arm being apparently further than the optical arm. Roberts (1972) developed the “two-armed spiral shock” model (TASS) to explain these discrepancies. According to this model a shock develops along the inner edge of the Perseus arm where the gas encounters a minimum in the gravitational potential of the density wave. The shock has an amplitude of approximately  $20 \text{ km s}^{-1}$ . In this framework the main ridge of Perseus arm emission seen from  $-40 \text{ km s}^{-1}$  to  $-50 \text{ km s}^{-1}$ , depending on the longitude (c.f. Figure 6 of Normandeau et al. 1997), has been displaced from circular velocity by approximately  $20 \text{ km s}^{-1}$ . In this context the absorption gap in the W3 spectrum at  $-30 \text{ km s}^{-1}$  would be due to the *undisturbed* gas behind W3, the HII region itself being within or just past the layer of shocked gas at  $\sim -40 \text{ km s}^{-1}$  (Fig. 6c).

This is reminiscent of the streaming motion seen in other spiral galaxies, e.g. M83 (Lord & Kenney 1991) and M51 (Rand 1993 and references therein). In M51, the strong density wave has concentrated both the diffuse and dense gas along the inner edge of the spiral arm, coincident with the dust lane, in the collision front. The velocity shifts are quite large, as much as  $60\text{--}90 \text{ km s}^{-1}$  in the plane of the galaxy (Tilanus & Allen 1991). The density wave is much weaker in M83, resulting in less pronounced streaming motions ( $\sim 12 \text{ km s}^{-1}$  perpendicular to the spiral arm and  $\sim 0 \text{ km s}^{-1}$  parallel to it; Lord & Kenney 1991). The dust lane again lies along the inner edge of the spiral arm but in this case the molecular ridge is offset, some 300 pc downstream. Lord & Kenney speculate that the diffuse gas is compressed at the shock front, producing the dust lane, but that the molecular clouds pass through the front to form a broad distribution in the arm.

The Perseus arm lies somewhere between these two cases: the  $20 \text{ km s}^{-1}$  offset is essentially perpendicular to the spiral arm, implying a stronger shock than in M83 but weaker than in M51 where the perpendicular component is approximately  $64 \text{ km s}^{-1}$  (Lord & Kenney 1991). Heyer & Terebey (1998) studied the CO and infrared emission in the W3/W4/W5 region and found the bulk of the CO emission to be at velocities near  $-45 \text{ km s}^{-1}$ . They estimate that the minimum transit time for the interarm region requires an exceedingly long cloud lifetime ( $3\text{--}6 \times 10^9 \text{ yr}$ ), and, when combined with the arm-interarm contrast which they measure to be 28:1 for CO, this implies that the gas which enters the spiral arms is in the atomic phase. All this is more akin to the situation in M51 than in M83, with a pile-up of molecular material along the shock front, though the shock is weaker for the Perseus arm than in M51. It should be pointed out, however, that Heyer & Terebey

discounted the possibility that the gas at  $-40 \text{ km s}^{-1}$  was in fact showing streaming motion.

Frail & Hjellming (1991) presented an absorption spectrum towards LSI+61°303, a Perseus arm object located just east of W4. It is very similar in appearance to the one presented here for W3, and they also called upon the TASS model to explain their observations. A large scale phenomenon such as a spiral density wave seems the most likely explanation for the similar velocity displacement of gas separated by some 78 pc (assuming a distance of 2.3 kpc). Frail & Hjellming also show a spectrum toward an extragalactic source, BG 0237+61 which is 15 arcmin from LSI+61°303, where there is absorption in the  $-20 \text{ km s}^{-1}$  to  $-40 \text{ km s}^{-1}$  velocity interval; this argues against the possibility outlined in §3.2.1. For these reasons, the explanation involving the TASS model is the one favoured here.

## 4. Discussion of optical depth and spin temperature

### 4.1. Absorption near $0 \text{ km s}^{-1}$

Of the HI studies towards W3 mentioned in the introduction, only the earlier ones cover a wide-enough velocity range to include the absorption by Local gas. Crovisier et al. found that the optical depths and widths of the troughs for W3 N and W3 “main” were comparable. The present data show slight differences. The optical depth towards W3-W rises and falls smoothly, attaining at maximum of  $0.66 \pm 0.08$  at  $-0.53 \text{ km s}^{-1}$ , whereas towards W3-N there is a brief plateau, extending over some  $8 \text{ km s}^{-1}$ , at a level of 0.6–0.7. Read also found a peak optical depth of  $\sim 0.6$ . Within the two subregion there is little variation.

The spin temperature towards W3-N attains slightly lower values than towards W3-W and remains at this level over a wider velocity interval, corresponding to the  $8 \text{ km s}^{-1}$  plateau mentioned above. Both sight-lines show slightly lower  $T_s$  (as low as  $99 \pm 19 \text{ K}$  towards W3-N and  $115 \pm 20 \text{ K}$  towards W3-W) than found by Wendker & Wrigge towards DR 7 (generally around 140 K). Considering the uncertainties, the discrepancy is not large. Nonetheless a possible explanation for this could be that the presence of relatively small, colder HI “clumps” would have a much greater impact on the spin temperatures measured towards W3 than towards DR 7. This is because for each channel only a mean brightness temperature is measured and, due to Galactic rotation, the same channel width (velocity width) corresponds to a greater path length for the DR 7 case than for W3. For DR7 sight-lines each channel would therefore include contributions from much warm gas as well



as from the postulated small, cold clumps. As an illustration, for  $v_{\text{LSR}} = -10 \text{ km s}^{-1}$  and assuming a flat rotation curve with an Oort constant  $A = 14 \text{ km s}^{-1} \text{ kpc}^{-1}$  and  $R_0 = 8.5 \text{ kpc}$ , one finds  $d_{\text{kin}} = 4.5 \text{ kpc}$  for the longitude of DR 7, but only  $0.7 \text{ kpc}$  for sight-lines towards W3<sup>1</sup>.

#### 4.2. Between the $0 \text{ km s}^{-1}$ and $-20 \text{ km s}^{-1}$ absorption troughs

In the interval between the troughs at  $0$  and  $-20 \text{ km s}^{-1}$ , Figure 2 indicates that there is some absorption, though not to the extent seen in the deep troughs. The optical depth calculations reach minima of  $0.14 \pm 0.03$  towards W3-W and  $0.08 \pm 0.04$  towards W3-N. It is reasonable to wonder if this is truly due to interarm absorption or if it is simply attributable to the overlap of wings from the distributions corresponding to the  $0$  and  $-20 \text{ km s}^{-1}$  troughs. Fitting a Gaussian to each of these shows that their wings cannot account for the amount of absorption seen at intervening velocities.

For both sight-lines, the spin temperature increases upon leaving the Local Arm. The rise and fall of  $T_s$  in this interarm region is fairly smooth towards W3-W, reaching  $286 \pm 79 \text{ K}$  when using the average absorption spectrum. Towards W3-N the interarm spin temperature shows a double peak, though it is smooth within uncertainties.

The above temperatures are, of course, weighted mean values for a given channel. They correspond to what Kulkarni & Heiles (1988) dubbed the *naively derived spin temperature*. For a single, isothermal cloud, it is equal to that cloud’s spin temperature, however for the more complicated and realistic case where there are contributions from two optically thin components, it becomes the column-density-weighted harmonic mean temperature. Assuming the canonical values of  $80 \text{ K}$  and  $8000 \text{ K}$  for the Cold Neutral Medium (CNM) and the Warm Neutral Medium (WNM) respectively (Kulkarni & Heiles 1988) and using  $300 \text{ K}$  as the value for the weighted harmonic mean spin temperature, one derives a column density that is three times as high for the WNM as for the CNM. From the measured values of the spin temperature and the optical depth in the  $-8.78 \text{ km s}^{-1}$  to  $-13.72 \text{ km s}^{-1}$  velocity interval, the total column density of the HI  $3.4 \times 10^{20} \text{ cm}^{-2}$ , implying a column density of  $8.4 \times 10^{19} \text{ cm}^{-2}$  for the CNM and  $2.5 \times 10^{20} \text{ cm}^{-2}$  for the WNM with the above assumptions. If one then uses as a path length the difference between the kinematic distances associated with the velocities given above ( $0.63 \text{ kpc}$  and  $0.96 \text{ kpc}$ ), one finds mean densities of  $0.08 \text{ cm}^{-3}$  for the CNM and  $0.24 \text{ cm}^{-3}$  for the WNM. The ISM pressure

---

<sup>1</sup>Kinematic distances can be calculated for this local gas because it is unaffected by the Perseus streaming motions.

in the plane is thought to be approximately  $\frac{P}{k} \sim 4000 \text{ cm}^{-3} \text{ K}$  (Kulkarni & Heiles 1988), implying  $n_{\text{WNM}} = 0.5 \text{ cm}^{-3}$  and  $n_{\text{CNM}} = 50 \text{ cm}^{-3}$ . Taking the ratio of the mean densities for the interarm velocities considered here and the expected densities in the plane, one finds volume filling factors  $\sim 50\%$  for the WNM and  $\sim 0.2\%$  for the CNM. The WNM filling factor is comparable to the value of  $\sim 40\%$  which Carilli et al. (1998) found for the average of two interarm regions along a line of sight towards Cyg A, though using only their data for the interarm region between the local gas and the Perseus arm results in a somewhat lower value, closer to 30%.

The CNM and WNM filling factors calculated above are very uncertain, relying as they do on many assumptions. The temperatures adopted for the two components may be incorrect. Carilli et al. measured temperatures for the WNM down to  $4800 \pm 1600 \text{ K}$ . While using this lower value would not noticeably change the mean densities derived for the two components in the interarm region, it would greatly affect the expected density for the plane and would imply a filling factor of  $\sim 30\%$  for the WNM. The CNM filling factor would, of course, be unaffected. The temperature chosen for the CNM has a greater impact on the implied relative column densities of the two phases; for  $T_{\text{CNM}} = 20 \text{ K}$ , the filling factor of the WNM becomes  $\sim 60\%$ , while for the CNM it is then below 0.1%. Deriving path lengths from the kinematic distances can only give rough estimates. Small differences in this number will result in widely differing estimates of the filling factor for the WNM ( $\sim 30\%$  for  $\ell = 0.5 \text{ kpc}$  and  $\sim 80\%$  for  $\ell = 0.2 \text{ kpc}$ ), though the CNM filling factor remains at the 0.1–0.2% level. Clearly, the greatest uncertainty comes from the densities assumed for the two components in the plane. These are affected by the temperatures as noted above, but also depend on the assumption that the phases of the ISM are in pressure equilibrium<sup>2</sup>, as well as on the reliability of the equation. The quantitative results quoted in the preceeding paragraph are therefore not to be blindly trusted, particularly for the WNM, however the calculations clearly and reliably show that the CNM occupies a negligible fraction of the interarm region. Nonetheless this small amount of cold gas dominates the absorption signal.

### 4.3. Absorption near $-20 \text{ km s}^{-1}$

Crovisier et al. interpreted their observations at these velocities as due to the presence of a large inhomogeneous cloud at a distance of approximately 1.5 kpc. In the context of the TASS model favoured here, the difference between sight-lines towards W3-N and W3-W

---

<sup>2</sup>The expression for the pressure was derived for the Warm Ionized Medium and can only be applied to other components if there is pressure equilibrium

is due to inhomogeneities in the gas on the near side of the Perseus Arm.

Towards W3-N the average optical depth rises and falls quickly, reaching only  $0.49 \pm 0.07$  at  $-20.32 \text{ km s}^{-1}$ . For the W3-W line-of-sight, the rise is more gradual than the decline and the maximum attained is much greater,  $1.66 \pm 0.26$  at  $-20.32 \text{ km s}^{-1}$ . Read found a peak optical depth of  $\sim 1.4$  for this trough, in agreement with the value above. Accordingly, sight-lines towards W3-W reach lower spin temperatures ( $69 \pm 13 \text{ K}$  for the average profile) than do those towards W3-N ( $119 \pm 23 \text{ K}$  for the average profile).

The optical depth is fairly uniform over the individual regions. A few anomalously high values (up to 2.6) do result from the calculations but these are correlated with steep gradients in the continuum image and are therefore likely to be artefacts. Two factors which could have affected these pixels are: 1) slight misalignments of the continuum and spectral line images, which would have a great impact on calculations in these steep gradient regions, are not impossible as the continuum image was selfcalibrated; 2) the gridding of the continuum image and of the spectral cube were done separately and both have been regridded, which procedure could have caused mismatches between the two data sets in steep gradient regions. Because the affected region is very near the field centre, bandwidth smearing is not a likely cause of these errors.

#### 4.4. Absorption near $-40 \text{ km s}^{-1}$

As indicated in the introduction, the absorption at velocities near  $-40 \text{ km s}^{-1}$  has been studied with the WSRT at higher spatial and spectral resolutions (Goss et al. 1983, and van der Werf & Goss 1990). A new detailed analysis of the HI associated with the various compact HII regions using the DRAO data is therefore not warranted, but a few aspects shall be addressed and discussed.

For the W3-N region, the lower limit for the maximum value using the average spectrum is 1.6. The optical depth varies little over the region; for the pixel by pixel calculations, a lower limit of 2.9 on the maximum optical depth was found at a velocity of  $-40.11 \text{ km s}^{-1}$ .

For this region Goss et al. calculated values up to 2.5 whereas Read found  $\tau$  up to  $\sim 8$ . The former are inconsistent with the present data. The latter may be overestimated due to poor continuum subtraction leading to an underestimate of  $T_{b,on}$  (Read did not have channels perfectly devoid of continuum at his disposal for continuum subtraction and estimated that this may have resulted in a 10 K oversubtraction). It is possible that the Westerbork results have underestimated the optical depth. The WSRT has a shortest baseline of 36 m and, as a result, the largest scale structure that can be imaged is  $\sim 10$

arcmin in extent. This filtering property of the array highlights small scale knots, and therefore would not affect the absorption spectra because the structure of the absorbing sources is on scales smaller than 10 arcmin (c.f. Figure 1). If all the HI emission was on scales greater than 10 arcmin then there would be no surrounding HI emission which would need to be accounted for through an off-source spectrum. However if the interferometer has not filtered out all of the HI emission, then neglecting it, as did Goss et al., will result in an underestimate of  $\tau$ . The W3-N opacity images published by van der Werf & Goss show values of  $\geq 4$ ; their calculations were done differently than those of Goss et al., circumventing the possible difficulty with  $T_{b,off}$  (see van der Werf & Goss 1989 for details of the method).

It should also be noted that for these velocities, it is likely that the optical depths derived here are also underestimated. This is because there is probably local HI associated with the W3 region itself which will not be accounted for in the “off” spectrum. The latter will therefore contain less HI emission at these velocities than would a spectrum towards the source if there were no absorption.

Spatial variations are much more marked in W3-W which, contrary to W3-N, is made up of several distinct HII regions. In particular, the highest values are attained towards W3 core (lower limit of 4.7 at  $-38.46 \text{ km s}^{-1}$  whereas the lower limit for the maximum from the average spectrum is 2.4), and lesser but marked enhancements are seen towards W3 K and W3 J as well as in the southern section of NGC 896. Again Goss et al. obtained slightly lower values, with a maximum of 4.0 being detected towards W3-A and W3-B. However van der Werf & Goss found  $\tau > 5.0$  towards all continuum sources and explained the discrepancy in terms of beam dilution; this reconciles the two Westerbork data sets, though beam dilution should cause the optical depth evaluated with the DRAO data to be even lower. As for Read, once again he quotes a higher value (lower limit of 9.0), but the same warning applies as for W3-N.

The average spin temperature is fairly constant over the entire velocity range of the absorption trough, for both W3-N and W3-W, at somewhat less than 100 K. This temperature is consistent with expected values for cores of Giant Molecular Clouds (20 – 100 K, Turner 1988).

## 5. Summary and conclusions

HI spectra towards W3-N and W3-W for velocities ranging from  $+55 \text{ km s}^{-1}$  to  $-154 \text{ km s}^{-1}$  have been presented. These were combined with an average spectrum for nearby

positions to calculate the optical depth and spin temperature for velocities where there was absorption of the continuum emission.

There is a lack of absorption around  $-30 \text{ km s}^{-1}$  which may be indicative of temperatures in excess of  $10^4 \text{ K}$  in the interarm region or which might correspond to gas behind the W3 region even though there is absorption out to  $-50 \text{ km s}^{-1}$ . In the latter case, it could be that the  $-30 \text{ km s}^{-1}$  gas has been displaced by  $\geq 19 \text{ km s}^{-1}$  from the standard rotation curve, or that it is the gas showing absorption near  $-40 \text{ km s}^{-1}$  that has been accelerated by a spiral shock in accordance with the Two Armed Spiral Shock model (Roberts 1972). Considering that Frail & Hjellming (1991) observe a very similar spectrum towards LSI+61°303, a source east of W4, the explanation wherein the  $-30 \text{ km s}^{-1}$  gas has been displaced seems the least probable. The explanation involving the TASS model is favoured here because of the unlikely absence of cold HI over the velocity span of the  $-30 \text{ km s}^{-1}$  feature.

For the Local Arm, the sight-lines presented here yield lower spin temperature values than reported by Wendker & Wrigge (1996) towards DR 7. This discrepancy may be due to the longer path length corresponding to each channel width for the earlier study. Additional investigations of this nature, towards other Galactic plane HII regions seen in the CGPS data, will clarify the matter. For the interarm region, values on the order of 300 K are found, from which one can estimate volume filling factors of  $\sim 50\%$  for the WNM and  $\ll 1\%$  for the CNM; the calculations require many assumptions and the number quoted for the warm HI cannot be said to be reliable, but the result for the CNM filling factor is quite robust. The  $-20 \text{ km s}^{-1}$  absorption trough which shows lower temperatures is part of the Perseus arm in the TASS model, not the interarm region.

The study of this second line of sight towards a Galactic plane HII region, following on work by Wendker & Wrigge towards DR7, confirms the usefulness of such studies both in determining characteristics of the ISM and in examining elements of Galactic structure. The many HII regions within the  $73^\circ$  longitude span of the CGPS should help us map the temperature and optical depth in the Galaxy.

The author is grateful to H.J. Wendker and C. Heiles for useful comments on previous drafts, as well as to an anonymous referee for comments helpful in the preparation of the final manuscript. The Dominion Radio Astrophysical Observatory’s synthesis telescope is operated by the National Research Council of Canada as a national facility. The Canadian Galactic Plane Survey is a Canadian project with international partners, and is supported by a grant from the Natural Sciences and Engineering Research Council of Canada.

Table 1. Components of the W3 region

Name	( $l, b$ )	Approx. size	Description
W3 North (W3-N)	(133.78, +1.42)	$9.5' \times 8.5'$	Evolved HII region
W3 “main”	(133.79, +1.18)	$16.5' \times 14.0'$	All the bright emission south of W3-N
W3 East (W3-E)	(133.81, +1.18)	$9.5' \times 14.0'$	Part of W3 “main”. Fan-shaped, lower intensity evolved HII region
W3 West (W3-W)	(133.72, +1.17)	$6.0' \times 10.0'$	Part of W3 “main”. Bright western emission
W3 core	(133.71, +1.22)	$4.5' \times 3.5'$	Part of W3-W. Bright northern sources
W3 A+B	(133.72, +1.22)	$< 1'$	Part of W3 core. Unresolved HII regions
W3 H+C+D	(133.69, +1.22)	$< 1'$	Part of W3 core. Unresolved HII regions
W3 K	(133.73, +1.18)	$< 1'$	Part of W3-W. Compact HII region south of W3 core
W3 J	(133.70, +1.17)	$< 1'$	Part of W3-W. Compact HII region south of W3 core
NGC 896	(133.70, +1.14)	$4.5' \times 6.0'$	Part of W3-W. Large ring south of W3 core

<sup>a</sup>Sizes are approximate, being dependant on the threshold used to determine the boundary of a particular region. They are given here to help the reader associate the names listed with the features seen in Fig. 1, and correspond roughly to the lowest closed contour  $\geq 20\text{K}$  around a given source. It should be noted in particular that W3-E could be said to extend further east than suggested by the dimensions given above.

<sup>b</sup>In this paper, W3 East (or W3-E) is used to refer to the fainter emission east of W3 “main”; this is the standard naming convention for low and intermediate resolution centimeter observations. It is important to point out that in infrared studies, W3 East often refers to the eastern of the two far-infrared sources in W3 “main”. Also, higher resolution radio studies sometimes refer to a component of W3 “main” as W3 E.

Table 2. Observational parameters for the spectral line data

Parameter	Value
ST primary beam	Gaussian, FWHM = 103 arcmin
ST baselines	12.858 m to 604.336 m, increment = 4.286 m
Spatial resolution	$1.00' \times 1.10'$ (EW $\times$ NS)
Polarisation	RR
Bandwidth	1 MHz
Central velocity (LSR)	$-50.0 \text{ km s}^{-1}$
Velocity coverage	$211 \text{ km s}^{-1}$
Channel width	$2.64 \text{ km s}^{-1}$
Channel separation	$1.65 \text{ km s}^{-1}$
ST sensitivity at field centre	3.0 K

## REFERENCES

- Carilli, C.L., Dwarakanath, K.S., Goss, W.M. 1998, ApJ, 502, L79
- Crovisier, J., Fillet, R., Kazès, I., Baudry, A. 1975, A&A, 45, 97
- Campbell, M.F., Butner, H.M., Harvey, P.M., Evans, N.J., II, Campbell, M.B., Sabbey, C.N. 1995, ApJ, 454, 831
- Frail, D.A., Hjellming, R.M. 1991, AJ, 101, 2126
- Goss, W.M., Retallack, D.S., Felli, M., Shaver, P.A. 1983, A&A, 117, 115
- Heyer, M.H., Terebey, S. 1998, ApJ, 502, 265
- Hofner, P., Churchwell, E. 1997, ApJ, 486, L39
- Kulkarni, S.R., Heiles, C. 1988, in *Galactic and Extragalactic Radio Astronomy*. Verschuur & Kellermann, eds. Springer-Verlag.
- Lloyd, S.D., Kenney, J.D.P. 1991, ApJ, 381, 130
- Normandeau, M., Taylor, A.R., Dewdney, P.E. 1997, ApJS, 108, 279
- Rand, R.J. 1993, ApJ, 410, 68
- Read, P.L. 1981, MNRAS, 194, 863
- Roberts, D.A., Crutcher R.M., Troland T.H. 1997, ApJ, 479, 318
- Roberts, W.W. 1972, ApJ, 173, 259
- Roelfsema, P.R., Goss, W.M. 1991, A&AS, 87, 177
- Sullivan, W.T., Downes, D. 1973, A&A, 29, 369
- Tieftrunk, A.R., Gaume, R.A., Claussen, M.J, Wilson, T.L., Johnston, K.J. 1997, A&A, 318, 931
- Tilanus, R.P.J., Allem, R.J. 1991, A&A, 244, 8
- Turner, B. 1988, in *Galactic and Extragalactic Radio Astronomy*. Verschuur & Kellermann, eds. Springer-Verlag.
- van der Werf, P.P., Goss, W.M. 1990, A&A, 238, 296



van der Werf, P.P., Goss, W.M. 1989, A&A, 224, 209

Wendker, H.J., Wrigge, M. 1996, A&A, 305, 592

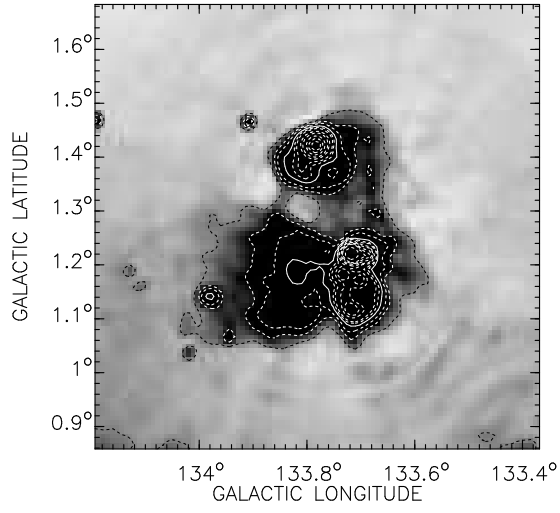


Fig. 1.— The W3 region at 1420 MHz. The greyscale varies from 0 K to 20 K. The solid line contour is at 50 K and the dotted contours are at 10, 20, 30, 70, 90, 150, 200, 300, 400, 500 and 1000 K.

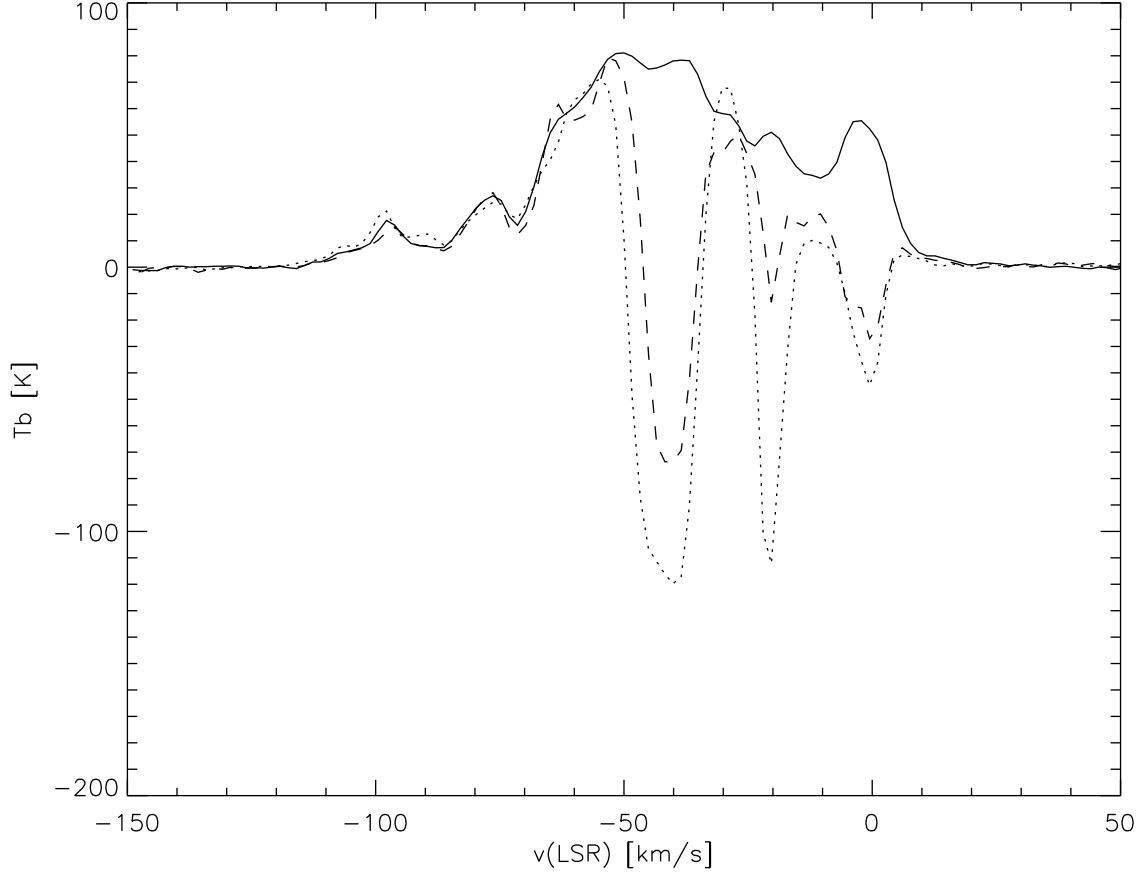


Fig. 2.— Absorption of W3-N and W3-W. HI spectra along lines of sight towards W3-N (dashed line) and W3-W (dotted line) are plotted along with the average emission spectrum of the surrounding gas (from an average of 40 nearby positions, see text). The absorption spectra were obtained by averaging the HI images for all pixels for which the continuum values were greater than 50 K, at the positions of W3-N and W3-W.

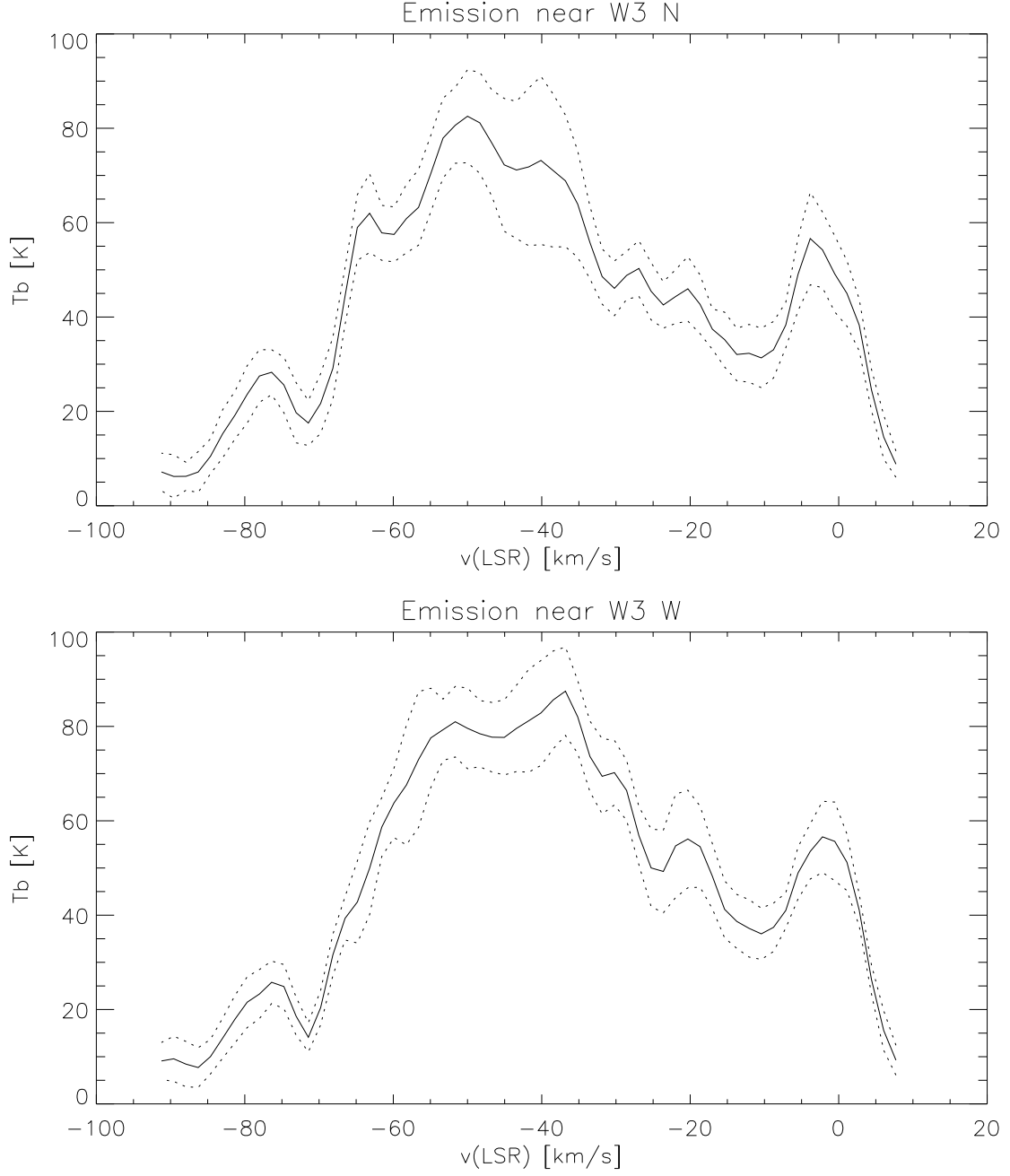


Fig. 3.— Average emission spectra towards W3-N and W3-W. A sample of twenty nearby positions for both W3-N and W3-W were used to derive the average emission spectra shown by the solid lines. The dotted lines are at plus and minus  $1\sigma$  from these average curves.

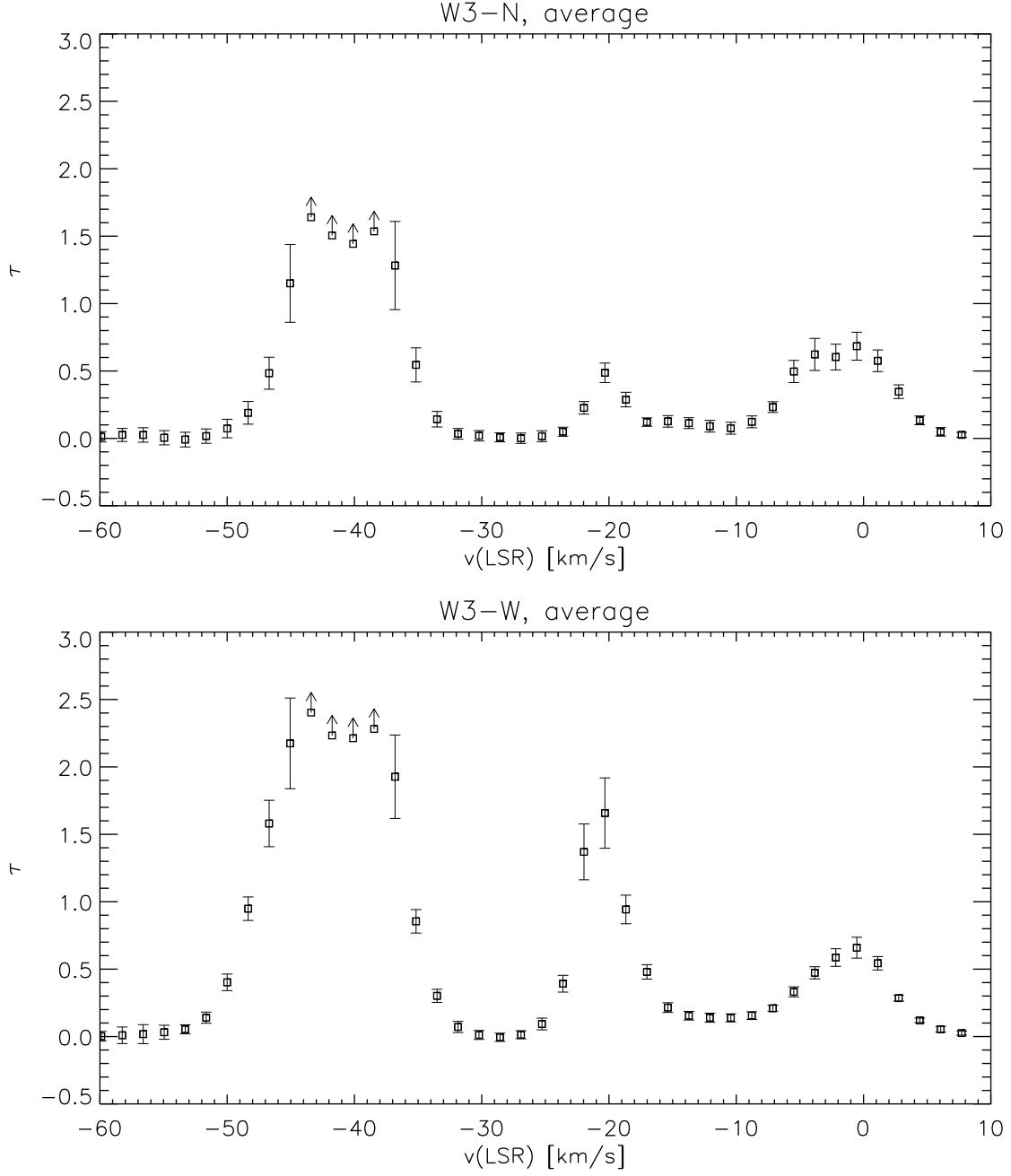


Fig. 4.— The optical depth profiles towards W3-N and W3-W. These were calculated using the on-source profiles shown in Fig. 2, i.e. the average spectra towards W3-N and W3-W, and the off-source spectra shown in Fig. 3. The points for which lower limits are indicated correspond to velocities for which  $T_{\text{off}} - T_{\text{on}}$  is within  $2(\sigma_{\text{off}} + \sigma_{\text{on}})$  of  $T_c$ .

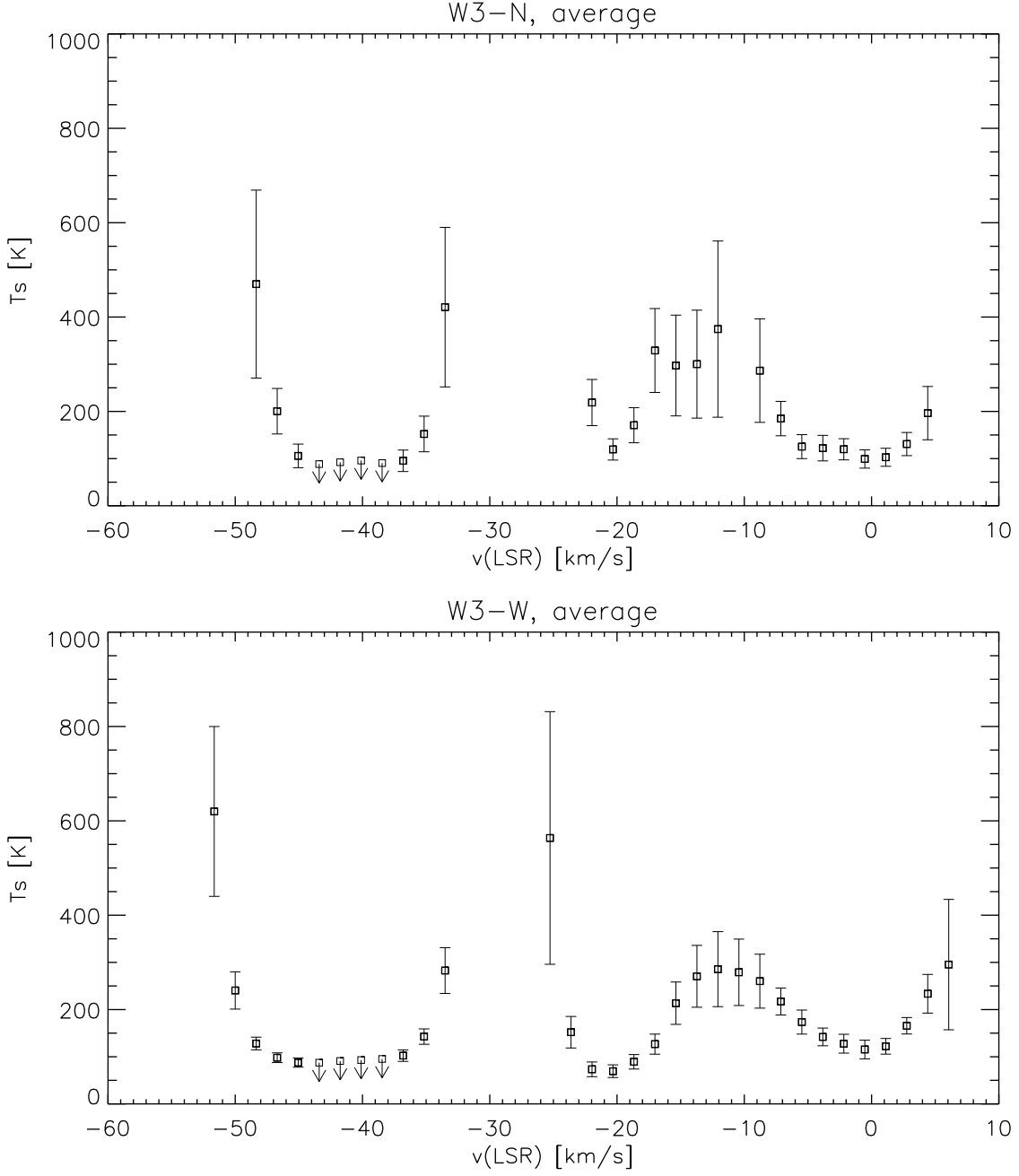


Fig. 5.— The spin temperature profiles towards W3-N and W3-W. These were calculated using the optical depth values plotted in Fig. 4, and the off-source spectra shown in Fig. 3. The points for which upper limits are indicated correspond to velocities for which only lower limits were calculated for  $\tau$ . Data points are only plotted for those channels where the calculated spin temperature was more than twice its uncertainty.

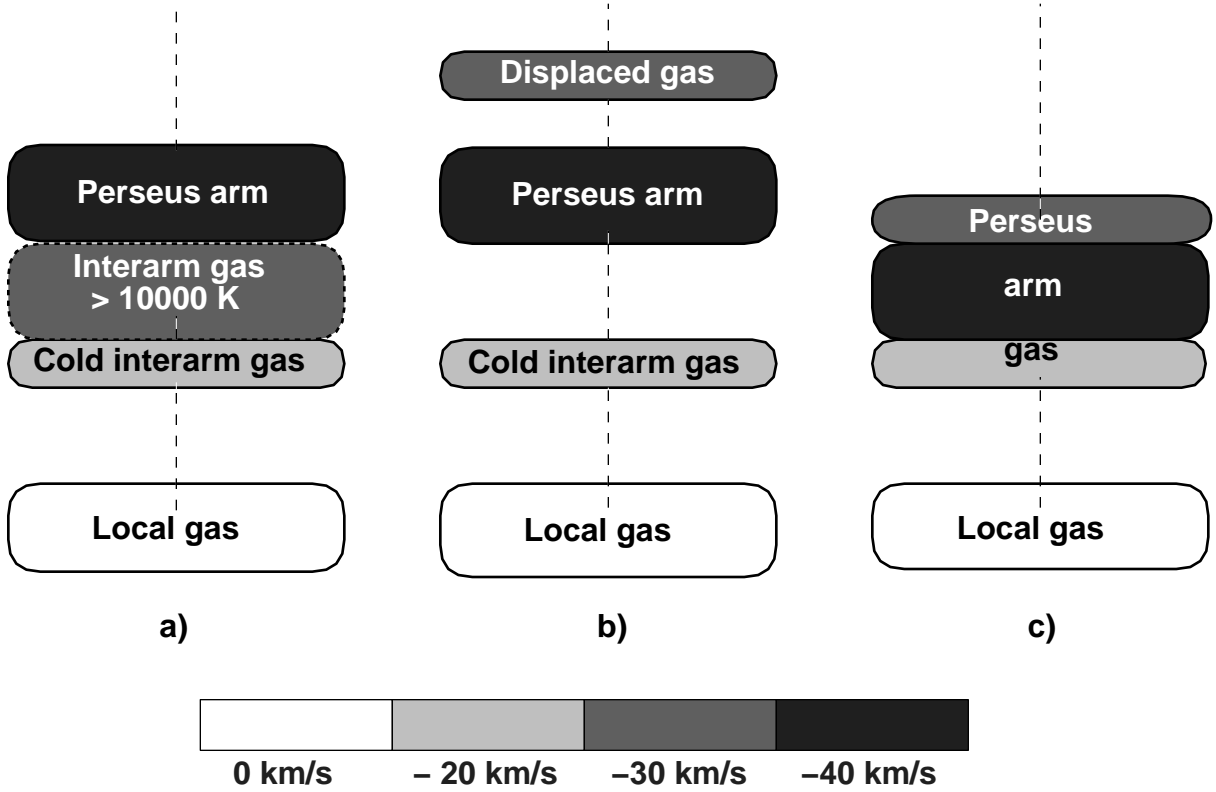


Fig. 6.— Schematic representation of the three explanations considered for the lack of absorption at  $-30 \text{ km s}^{-1}$ . The diagrams are not to scale. a) There is no absorption by the interarm gas around  $-30 \text{ km s}^{-1}$  even though it is in front of W3. This implies spin temperatures in excess of  $10^4 \text{ K}$  which is unlikely for warm, neutral gas. b) The gas at  $-30 \text{ km s}^{-1}$  is behind W3 but is not following the rotation curve. c) The gas at  $-40 \text{ km s}^{-1}$  is shocked gas in the Perseus arm whereas the gas at  $-30 \text{ km s}^{-1}$  is unshocked gas in the Perseus arm. This is the picture suggested by the TASS model (Roberts 1972).